Thesis for the degree of Doctor of Philosophy

Time Domain Systems for Microwave Imaging: Accuracy Evaluations and Prototype Design

Xuezhi Zeng

CHALMERS

Department of Signals and Systems
Biomedical Electromagnetics Group
Chalmers University of Technology
Göteborg, Sweden 2013

Time Domain Systems for Microwave Medical Imaging:
Accuracy Evaluations and Prototype Design
Xuezhi Zeng
ISBN 978-91-7385-925-7

Doktorsavhandlingar vid Chalmers tekniska hoskola
Ny serie nr 3606
ISSN 0346-718x

Department of Signals and Systems
Biomedical Electromagnetics Group
Chalmers University of Technology
SE–412 96 Göteborg
Sweden
Telephone +46–(0)31–772 10 00

Cover: The figure shows a picture of the developed prototype.

Printed by
Bibliotekets Reproservice
Chalmers Tekniska Högskola
Göteborg, Sweden 2013

To my husband Xi Cheng, and my beloved son Qiyou

Abstract

This thesis focuses on microwave hardware development for medical applications. In this thesis, we have evaluated the accuracy of time domain systems for medical imaging, and a time domain system dedicated to medical imaging has been designed, developed and tested.

As a potential imaging modality for biomedical applications, microwave medical imaging has attracted a lot of attention in recent years. Most of the ultra wideband microwave imaging systems reported so far are based on commercial instruments, which are only appropriate for experimental purpose due to the high cost and big size. In order to speed up clinical trials, it is highly desirable to have a custom designed system with low cost, small size, high speed and enough accuracy.

With the development of solid state technology, time domain measurement technology has become more and more attractive for ultra-wideband applications. This is due to the low cost, high speed and simple structure.

The accuracy of time domain systems is the main concern for the use in medical applications. In the first part of the thesis, we studied the accuracy issue of time domain systems. Theoretical analysis was performed to estimate the measurement accuracy and the results were verified by simulations and experiments. An imaging study was performed in order to compare the image reconstructions obtained by using a time domain experimental system and an ultra wideband frequency domain system respectively, with comparable results in the permittivity reconstructions. The study of a high contrast breast model showed that when the amplitude uncertainty and phase uncertainty of measurements were less than 1.5 dB and 15 degrees, the effects of noise on reconstructed images were small.

Based on the investigations and current technology limitations, we proposed a time domain system design dedicated to microwave medical imaging. A prototype was developed and its measurement accuracy was evaluated. An imaging test was also performed with the prototype and the results were compared with those obtained using our experimental system. The imaging results demonstrated the capability of the developed system for imaging.

Keywords: Microwave Imaging, Ultra-Wideband, Time Domain Measurement, Frequency Domain Measurement, Medical applications, Accuracy, Equivalent Time sampling, Real Time sampling.

Acknowledgements

I would like to express my sincere gratitude to those who have helped me a lot during my PhD study. Firstly I would like to thank my examiner Prof. Herbert Zirath for giving me the opportunity to work on such an interesting project between two different departments. I'm also grateful to his thoughtful comments and suggestions. My biggest thanks go to my main supervisor Prof. Mikael Persson. Thank him for creating such a pleasant research environment in the group. The joy and enthusiasm he has for research was contagious and motivational for me, especially during tough times in the PhD pursuit. I appreciate all his contributions of time, ideas and support. I'm especially grateful to my cosupervisor Docent Andreas Fhager, who always provides encouraging and constructive feedbacks to my papers and thesis. He has been actively interested in my work and has always been available to advise me. Docent Peter Linner, my cosupervisor in MC2, thanks a lot for the interesting discussions on microwaves and encouragements.

Many thanks to my colleagues in our research group for their kind help and support. Special thanks to Hana Dobsicek Trefna for her friendship. She is always there when I need help. Thanks to my previous colleague Markus Johansson for the interesting Electromagnetic problem discussions and for helping me frequently with the tough Swedish translation work. Thanks to Oskar Talcoth for always being willing to give me a hand when I need help.

I'm very grateful to my Chinese friends, who help me a lot in the past six years. Many names need to be mentioned here, Jingya Li, Gongpei Cui, Zhennan Fei, Xiaoming Chen, Yutao Sui, Tong Ning, Wanlu Sun, Wei Yang, Xinlin Zhang, Yinan Yu etc. Special thanks to Jiangya Li, Gongpei Cui and Yutao Sui, thank you for helping me going through difficult times. Life would be boring and tough without your friendship and help.

I want to thank Ann-Christine Lindbom, Madeleine Persson and Agneta Kinnander for giving me a lot of help on my study, teaching and research. I also want to thank Mattias Ferndahl and Kristoffer Andersson for helping me with the experiment system arrangement in MC2. I would also like to take this opportunity to appreciate the help I got from other colleagues in

S2 and MC2.

Last, but not least, I would like to dedicate this thesis to my family, my husband Xi Cheng and my beloved son Qiyou.

List of publications

Appended papers

The thesis is based on the work contained in the following papers.

Paper A
X. Zeng, A. Fhager, M. Persson, P. Linner and H. Zirath, "Accuracy Evaluation of Ultrawideband Time Domain Systems for Microwave Imaging," *IEEE Trans. Antennas Propagat.*, vol. 59, no. 11, pp. 4279–4285, 2011.

Paper B
X. Zeng, A. Fhager, P. Linner, M. Persson and H. Zirath, "Experimental Investigation of the Accuracy of an Ultrawideband Time-Domain Microwave-Tomographic System," *IEEE Trans. Instrum. Meas.*, vol. 60, no, 12, pp. 3939–3949, 2011.

Paper C
X. Zeng, A. Fhager, P. Linner, M. Persson and H. Zirath, "Design and Performance Evaluation of a Time Domain Microwave Imaging System," *International Journal of Microwave Science and Technology*, Manuscript Accepted for Publication, 2013.

Paper D
X. Zeng, A. Fhager, Z. He, M. Persson, P. Linner, and H. Zirath, "Development of a Time Domain Microwave System for Medical Diagnostics," Submitted to *IEEE Trans. Instrum. Meas.,* 2013.

Other papers

The papers listed below in chronological order overlap with the appended papers or are not in the main focus of the thesis.

[1] X. Zeng, A. Fhager, P. Linner, M. Persson and H. Zirath, "Accuracy Evaluation of Time Domain Measurement Systems for Microwave Tomography," *IEEE MTT-S Int. Microwave Symp. Dig.*, pp. 1441–1444, Jun. 2009.

[2] X. Zeng, A. Fhager, P. Linner, M. Persson and H. Zirath, " Time Domain System for Microwave Tomography," *Medicinteknikdagarna 2008*, Sep. 2008.

[3] M. Persson, A. Fhager, H. Dobsicek Trefna, and X. Zeng, " Broadband microwave based diagnostics and treatment," *3rd European Conference on Antennas and Propagation*, March, 2009.

[4] X. Zeng, A. Fhager, and M. Persson, " Investigations on the System Measurement Uncertainty for Microwave Tomography," *Medicinteknikdagarna 2009*, Sep. 2009.

[5] X. Zeng, A. Fhager, and Mikael Persson, "Study on the Sensitivity of Image Reconstruction to the Measurement Uncertainty in Microwave Tomography," *4th European Conference on Antennas and Propagation*, April, 2010.

[6] A. Fhager, H. Dobsicek Trefna, X. Zeng, P. Linner, H. Zirath, J. Stake and M. Persson, "Clinical diagnostics and Treatment with Electromagnetic Fields," *4th European Conference on Antennas and Propagation*, April, 2010.

[7] X. Zeng, A. Fhager, P. Linner, M. Persson and H. Zirath, "Comparison between a time domain and a frequency domain system for microwave tomography," *Medicinteknikdagarna 2010*, Sep. 2010.

[8] X. Zeng, A. Fhager, P. Linner, M. Persson and H. Zirath, "Accuracy investigation of an ultra-wideband time domain microwave imaging system," *5th European Conference on Antennas and Propagation*, April, 2011.

[9] X. Zeng, A. Fhager, and M. Persson, " Influence of noise on breast tumor detection using microwave tomography," *Medicinteknikdagarna 2011*, Sep. 2011.

[10] X. Zeng, A. Fhager, M. Persson, P. Linner, and H. Zirath, "An ultra-wideband microwave medical diagnostic system: design considerations and system performance ," *6th European Conference on Antennas and Propagation*, March, 2012.

Contents

Abbreviations and acronyms

ADC	Analog to Digital Converter
AGC	Automatic Gain Control
AWG	Arbitrary Waveform Generator
DDS	Direct Digital Synthesizer
DSP	Digital Signal Processing
FFT	Fast Fourier Transform
FWHM	Full Width at Half Maximum
FPGA	Field Programmable Gate Array
IF	Intermediate Frequency
LNA	Low Noise Amplifier
LSB	Least Significant Bit
MWT	Microwave Tomography
NF	Noise Figure
OUT	Object under Test
PA	Power Amplifier
PLL	Phase Locked Loop
RF	Radio Frequency
RMS	Root Mean Square
RSS	Root Sum Square
SNR	Signal to Noise Ratio
T/H	Track and Hold
VCO	Voltage Controlled Oscillators
VNA	Vector Network Analyzer
UWB	Ultra-Wideband

Chapter 1

Introduction

1.1 Ultra wideband microwave medical imaging

Microwave imaging for medical applications has been extensively researched in the last years. Particularly, the use of ultra wideband (UWB) data for imaging is of special interest. With this technique, microwave signals are used to illuminate biological tissue, reflected or scattered fields are recorded and used for image reconstructions.

In this section, the subject of UWB microwave medical imaging is briefly introduced, mainly including the background, experimental imaging systems and conventional imaging approaches.

1.1.1 Background

In the past years, the use of microwaves for biomedical imaging has been extensively investigated [1]-[9]. With microwave imaging, biological tissues are differentiated based on differences in dielectric properties. It has been shown that the dielectric properties of biological tissues are strongly dependent on its physiological and pathological conditions [10]-[15]. For example, malignant tumors have higher permittivity and conductivity values than normal tissues due to a higher water content [16]-[18]. Therefore, microwave imaging has potential for many biomedical applications, such as breast tumor detection [4]-[5], [9], functional imaging [19] and thermal measurement [20] of biological tissues.

Microwave imaging methods can be based on monofrequency [2]-[4], multiple frequency [21]-[23], or UWB data (i.e. time-domain data) [5], [7]-[9]. The use of UWB data has been of particular interests to the research com-

munity due to its potential for high resolution imaging.

UWB refers to radio technology that employs a bandwidth greater than 20% of the center frequency or 500 MHz [24]. In practice, there are two commonly used UWB band for medical imaging. One is from 500 MHz to 3 GHz, and the other is allowed by the Federal Communication Commission (FCC) for indoor applications, i.e., 3.1 GHz to 10.6 GHz [24]. With the UWB illumination, more information about the object can be collected in comparison with a monofrequency case. Particularly, UWB technology constitutes a good tradeoff between penetration depth and spatial resolution for microwave medical imaging.

1.1.2 Experimental imaging systems

There are two main problems in UWB microwave imaging: accurate measurement of data and efficient use of this data for image reconstruction.

The measurement of UWB data could in principle be carried out in the frequency domain or in the time domain. It is straight forward to build a microwave imaging system based on commercially available instruments.

Most UWB microwave experimental systems for medical imaging work in the frequency domain and often these systems are based on commercially available vector network analyzers (VNAs)[7], [9], [25]-[29]. The VNA utilizes a step frequency technique to perform the measurement in a wide frequency range. Each time, a sinusoidal signal with different frequency is transmitted to illuminate the object under test (OUT) and the scattered signals are then received by the VNA, and scattering parameters are calculated. From this frequency domain scattering data any time domain pulse can be synthesized with a Fourier transformation [30]–[31]. A VNA is usually supported with a powerful measurement platform including matured calibration functions, which provides a ready use and high accurate measurement solution for experimental use.

There are also examples of experimental systems working in the time domain and they usually consist of a pulse generator and a sampling or high speed real time oscilloscope [32]–[35]. The operating principle for such system is that the pulse generator is used to generate a pulse to illuminate the OUT and the time domain response is measured with the oscilloscope. The sampling oscilloscope uses an equivalent time sampling technique which constructs a UWB signal based on measurements over several repetitive wave cycles, and this means that the signal must be repetitive. In the last few years, high speed real time oscilloscopes have become commercially available and they are capable of acquiring a pulse with single-shot measurement, this results in much faster measurement, which is very attractive for medical

applications.

1.1.3 Imaging approaches

After obtaining the object's response, an imaging algorithm reconstructs images from the measured data.

There are two main principles for the imaging algorithms: microwave tomography and radar based imaging. In principle, the same measurement configuration can be used for both imaging approaches and a typical measurement system consists of an antenna array which is used to transmit microwave signals into an OUT and receive scattered fields. Fig. 1.1 shows the measurement configuration of a typical imaging system. The black circles represent the transmitters/receivers surrounding the unknown object.

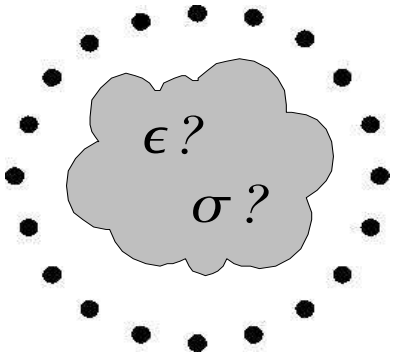

Figure 1.1: The measurement configuration of a typical imaging system. The black circles represent the transmitters/receivers surrounding the object under test.

Microwave tomography is an approach in which an inverse scattering problem must be solved. The scattered field is nonlinearly related to the inhomogeneity of the object due to the multiple scattering effect [36] and the nonlinear effect becomes more pronounced with an increasing contrast. The nonlinear problem is very computationally demanding to solve, and instead a class of algorithms have been developed where a linear approximation, such as the Born or Rytov approximations have been utilized [37]-[39]. These algorithms have been proven to be effective when imaging small and weakly scattering objects. However, these algorithms are of limited interests for biomedical applications as they fail to handle the large contrasts usually found in biological tissue [40]–[41]. With the increase in the computational capabilities, during the past few years several iterative nonlinear methods [4], [7], [42]-[46] have been explored for tomographic imaging. Reconstructions are

accomplished by iteratively comparing the measured data with numerically calculated data.

Most of the research work on microwave tomography investigated single frequency reconstructions. The use of monofrequency data at a high frequency often resulted in the inverse algorithm being trapped in local minima due to the highly nonlinear nature of the problem [47]. The multiple frequency approach was then proposed to overcome the local minima problem in order to achieve better reconstruction quality. It could be implemented either by a sequential use of the spectral data [21, 22] or by a concurrent use of several discrete frequencies [23]. With this approach, the lower frequency components aided in the linearization of the problem and the higher frequency components contributed to the spatial resolution. Unlike the multifrequency approach, which used only a few measurements at different discrete frequencies, a time domain inversion algorithm [7]–[8] utilized the information of the target over an entire band, which gave highly stable and high resolution reconstructions.

In contrast to microwave tomography, radar based imaging avoids complex image reconstruction algorithms and has been extensively investigated for biomedical applications, such as breast cancer detection. In this approach, a UWB signal is used to illuminate the breast and the scanning mode could be mono-static, bi-static and multi-static. The tumor response is utilized to identify the presence and location of significant scatters by means of delay-and-sum, space-time beam forming or data-adaptive focusing algorithms [25]-[29]. In order to apply these methods, tumor response must be extracted from received signals, which contain the tumor response, as well as additional signals, such as antenna coupling, reflections from the skin, scattered field from normal scatters (e.g, glandular tissue). The imaging results consequently relies on the cleanness of the tumor response.

1.2 Motivation and aim of the thesis

As mentioned before, the VNA has became the standard measurement device for UWB microwave imaging due to the high measurement accuracy over a very broad band and the easy operating platform. While commercial instruments provide ready solutions for experimental purposes, their high cost and massive size make these solutions unconvenient for practical use. In the development of more user friendly and commercially viable systems, it is desirable to have a custom-designed UWB microwave diagnostic system with compact size, low cost and high speed.

In many applications, such as microwave sensing and imaging, the fre-

quency band is almost always fixed and predefined. Therefore, one can partially abstain from the large flexibility of laboratory instruments in order to achieve simpler and integration friendly device concepts.

Frequency domain based UWB system, such as VNA, suffer from long settling time due to the need of narrowband filters or slow synthesizers. Hence, the measurement speed is quite limited. Moreover, the system is composed of sophisticated device modules, which often defy a monolithic integration. Therefore, time domain measurement technology is more promising when it comes to the design of a dedicated UWB system.

Large efforts have been devoted to developing low cost and compact UWB radar systems. Impulse based UWB radar transceivers are becoming commercially available and the Novelda impulse radar is one such [48]. It is a CMOS system integrated on a single chip, mainly targeting monitoring applications. Another example of efforts in the same direction is a time domain system developed for see-through-the-wall radar imaging based on field programmable gate array (FPGA) technology [49]. A major problem with such system is that the clocks generated by the FPGA suffer from significant timing jitter(tens of picoseconds RMS) [50], which limits the system's measurement accuracy. Recently, UWB pseudo-noise radar [51]–[52] has shown big potential. This type of system uses pseudo-random signals as stimulus and unlike an impulse radar system, the energy is now distributed over the whole transmission period. Therefore, with the same amplitude, better signal to noise ratio (SNR) can be obtained in comparison with impulse radars [53]. This system, however, is incapable of range gating [54] as the transmitted signal has a 100 % duty cycle. In addition, this system works more like a time domain VNA as a reference channel for measuring the stimulus is also needed.

To our knowledge, very little work has been done so far on hardware development for medical imaging. The complex measurement scenario (multiple antennas and lossy media) and requirements on the measurement accuracy is a real challenge in the system design. In this thesis, we have studied and developed a time domain system dedicated for medical imaging.

1.3 Content and outline of the thesis

The main content of the thesis work is summarized here: First, two different types of UWB measurement system are introduced, compared and contrasted. Their system structure and measurement principle are described. The advantages and disadvantages are discussed. Second, the accuracy of time domain systems, is investigated comprehensively. Third, the design

challenges of a time domain system for medical imaging is discussed. Accordingly, a dedicated system design is proposed and a prototype is developed and tested.

The thesis is divided into two parts. The first part provides the background needed for those not familiar with the subject and gives a brief introduction of the author's work. The second part includes the author's contribution in the form of appended papers. The outline of the first part is as following. Chapter 1 gives an overview of microwave imaging for medical applications. In Chapter 2, conventional UWB measurement technologies, mainly the system architectures and measurement strategies, are introduced and compared. The accuracy problem of time domain systems is investigated in Chapter 3. In Chapter 4, the proposed system design, developed prototype and test results are presented.

Chapter 2

Measurement Technologies

In UWB microwave imaging, the efficient measurement of an object's response to UWB excitation is of utter importance to the performance of the system. The measurement of UWB responses could be performed in several ways. In this chapter, two conventional technologies for UWB data measurement: frequency domain and time domain measurement technologies, are introduced. The system architectures and measurement strategies are described in detail.

2.1 Frequency domain measurement technology

Frequency domain measurement technology is commonly used for measuring the scattering response of microwave devices. Commercial VNA is a typical UWB measurement instrument based on this technology.

The principal system architecture of a UWB frequency domain measurement system is shown in Fig. 2.1. The measurement procedure is that the radio-frequency (RF) generator produces a sinusoidal test signal which illuminates the OUT and the response of the object at this frequency is recorded by the receiving antenna. The received signal is first amplified by using a low noise amplifier (LNA) and then down converted to an intermediate frequency (IF) component through a mixer for a more accurate processing. A narrow band IF filter is applied after the mixer to eliminate the interference signals at other frequencies. The output of the IF filter is sampled and digitized with an analog to digital converter (ADC) with high accuracy and the output digital data is then processed with a digital signal processing module (DSP).

By changing the frequency of the generated signal stepwise, the response

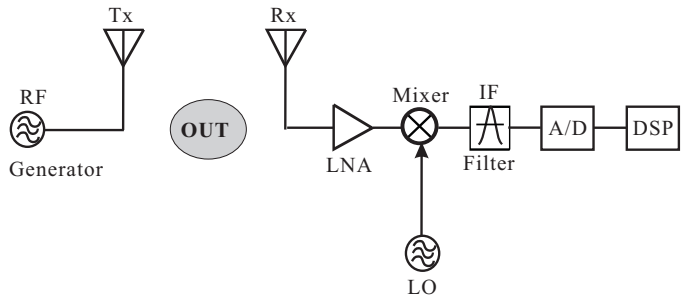

Figure 2.1: Principal system architecture of an ultra-wideband frequency domain measurement system for microwave imaging.

of the object at several discrete frequencies are obtained. By making the frequency interval small enough, the object response over a wide band is obtained approximately from the responses at many discrete frequencies by the means of interpolation.

The hardware and techniques most commonly used in such a system [55], are described below.

Generator The generator produces the sinusoidal stimulus signals with different frequencies. The core component is an electronically tunable oscillator with a relatively wide tuning range. To ensure the required frequency stability and spectral purity, it is embedded in a phase locked loop (PLL) [56]. A PLL links the frequency and phase of the tunable oscillator to the reference oscillator. This helps to improve the spectral purity of the tunable oscillator in the vicinity of the operating frequency. Using suitable techniques in the PLL, it is possible to modify the frequency ratio between the reference oscillator and the tunable oscillator in order to generate the frequencies needed for the stimulus signal. Implementation of the required tuning range with the tunable oscillator requires several switchable voltage-controlled oscillators (VCOs).

Receiver The receiver is usually based on the homodyne principle or the heterodyne principle, where the latter gives higher accuracy measurements. The heterodyne principle involves having a local oscillator whose frequency f_{LO} is different from the received frequency f_{RF}. This means that the received RF signal is converted to an intermediate frequency $f_{IF} = |f_{RF} - f_{LO}|$ signal, with the magnitude and phase of the RF signal retained. By choosing a suitable local frequency f_{LO}, any RF frequency within the receiver's range can

be converted to a fixed intermediate frequency. This simplifies the subsequent IF processing which is handled digitally in modern instruments.

The analog mixer is generally the component limiting the dynamic range. If the input level of the mixer is too high, it will produce nonlinear distortion. However, the linear range of the mixer is also not suitable for arbitrarily low-amplitude signals since the noise prevents measurement of very low-amplitude signals. Using an amplifier with tunable amplification, variations in the levels in the analog section of the receivers can be optimized for the current RF input level. The required amplification is determined during a fast preliminary measurement. This technique is known as automatic gain control (AGC).

Initial filtering is used at the intermediate frequency stage which helps to keep a large share of the received broadband noise out of the following signal processing chain. It also serves as an anti-aliasing filter for the ADC.

The analog to digital converters used in modern vector network analyzers works at a low frequency and generally have a resolution of at least 14 bits. Using additional techniques like dithering [57], it is possible to further increase their effective resolution.

2.2 Time domain measurement technology

As the use of UWB technology has been explored for a wider range of applications, there is an increased demand on the measurement speed.

As described above, wideband measurements performed in frequency domain requires sweeping a large number of discrete frequencies, which is time consuming. In comparison with a UWB frequency domain measurement technology, the time domain measurement technology has the inherent advantage of fast acquisition of UWB data, which make it attractive for medical applications.

The system block diagram of a typical UWB time domain measurement system for microwave imaging is shown in Fig. 2.2. A UWB pulse generated by the pulse generator is transmitted by the antenna to illuminate the OUT and the object's response is acquired by the receiving antenna. The received signal is sampled and digitized for use in the image reconstructions. One or more amplifiers may be used before the sampling and digitizing module in order to adjust the acquired signal to the optimal signal level. Depending on the sampling technique, the sampling and digitizing functions can be realized by one or more components.

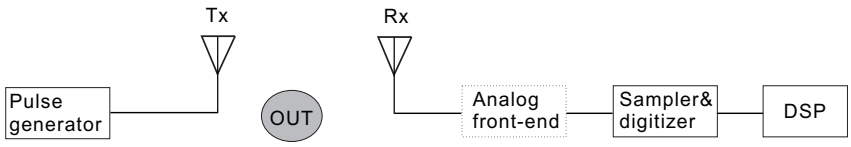

Figure 2.2: System block diagram of a time domain measurement system for microwave imaging

2.2.1 Pulse generation

A pulse generator is an essential component of a time domain UWB system. Common pulse shapes can be classified into categories: rectangular, Gaussian impulse, monocycle(differential Gaussian impulse), and step [58]. The shape of a pulse determines its spectral energy.

There are various pulse generation techniques. The four techniques of discrete RF transistor, avalanche transistor, step-recovery diode(SRD) and tunnel diode are classical and can be found in the scientific literature dating back to the 1960s [59]. Non-conventional techniques, such as custom designed nonlinear transmission lines(NLTLs) are specially used for the generation of ultra-fast rise time and high amplitude simultaneously [60].

The required bandwidth for microwave medical imaging corresponds to a pulse with duration less than hundred picoseconds(ps) according to the time-frequency relation. The two most commonly used techniques for the generation of pico-second pulses are SRD and NLTLs. SRD technique uses commercial, off-the-shelf, electronic components, therefore is simple and inexpensive, which makes it the most promising devices for UWB pulse generation. Many pulse generator designs reported for UWB applications are based on SRD [61]-[63]. However, the generated pulses have low amplitudes and a moderately high level of random jitter. Pulse generator built with custom designed NLTL generally have lower jitter, but are more complex in its design.

2.2.2 Data sampling

The most basic method of digitizing a waveform is to convert the instantaneous voltage level of the signal into a digital sample by using an ADC. Analog bandwidth and sampling rate are the two crucial parameters in choosing an appropriate ADC. The analog bandwidth of a system is a frequency range within which the system components are well matched and the mea-

sured signal is little distorted. In order to reconstruct a sampled waveform from stored digital samples, it is necessary that the rate of sequentially sampling and storing of the instantaneous signal levels is high enough. The minimum rate necessary to accomplish this is generally determined by the Nyquist rate, which should be at least twice as the signal bandwidth.

As long as the ADC's bandwidth covers the frequency range and it has the required sampling rate, the process of digital sampling can be realized with real-time sampling. In real time sampling, the ADC sequentially samples the input signal and the digital samples are stored in corresponding memory locations.

When these requirements can not be met, an equivalent time sampling technique is commonly used. In an equivalent time sampling system, a wide band sample and hold (S/H) or track and hold (T/H) component is usually used ahead of a low speed ADC. The received signal is sampled with the S/H or T/H and the output is kept constant for a period of time. In this way, even a very wide band signal can be measured with an ADC of moderate sampling rate. In other words, the equivalent time sampling technique relaxes the requirements on the speed of the ADC. Conventional digital circuitry, such as micro processors and memory devices, can be used to receive the digital samples and store them collectively as a time record for later retrieval and reconstruction of the input signal. In order to implement this technique, the measured signal should be repetitive.

In the following, the sampling process of both equivalent time sampling and real time sampling techniques are described.

Equivalent time sampling

The idea with equivalent time sampling is that the effective sample rate of analog to digital converter can be extended beyond the nominal sampling rate of the ADC. The basic requirements for equivalent time sampling are that the sampled signal should be repetitive and that a fixed starting point on the signal is known.

In equivalent-time sampling, a slow replica of the radio-frequency (RF) signal is assembled from individual measurements on many repetitions of the signal. There are two kinds of equivalent time sampling, namely, *random* equivalent-time sampling and *sequential* equivalent-time sampling. The principle of the *sequential* equivalent time sampling technique is illustrated in Fig. 2.3 [64] and a description of the *random* equivalent time sampling technique can be found in [65].

In the first measurement cycle, the amplitude of the signal is measured at the starting point $T = T_0$, which is marked as point (1) on the input

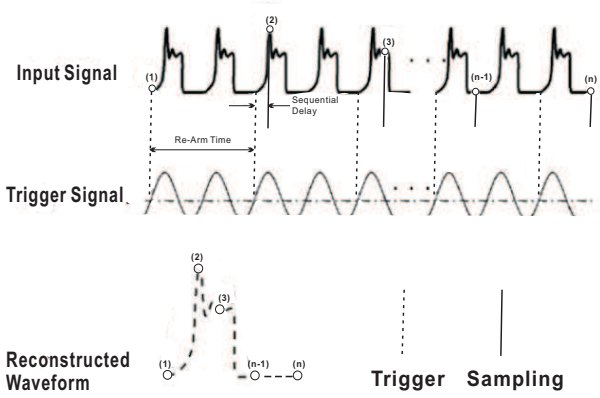

Figure 2.3: The principle of equivalent time sampling method

signal. Then a sequential delay, Δt, is added to the time base. In the second measurement cycle, the amplitude is measured at time $T = T_0 + \Delta t$, marked as point (2) on the input signal. In the third measurement cycle, the amplitude is measured at time $T = T_0 + 2\Delta t$, marked as point (3). The procedure is then repeated n times over n repetitions of the RF signal, until the entire pulse length has been samples with the desired sample rate. The samples are stored in corresponding locations in a digital acquisition memory. The sampled signal can then be constructed from the stored digital samples, as shown in the figure.

The equivalent time sampling technique usually utilizes sophisticated timing circuits which determine selected points on the signal at precisely calculated time intervals from the starting point of the repetitive signals. Fig. 2.4 shows the functional blocks of an equivalent time sampling module. The timing circuit is used to determine the exact timing of the sampling and the propagation delay between the sampler and the ADC need to be taken into account in order to make the ADC digitize the sampler ouput at the right position.

Real time sampling

A UWB time domain system with real time sampling captures an entire waveform on each trigger event. This means that a large number of data points are captured in one continuous record. This type of system usually use several high speed ADCs working in parallel and the samples collected from all the ADCs are interleaved to produce the output [66]. Fig. 2.5 shows the real time sampling process [64]. The real time sampling system can be triggered on a feature of the data itself, and often when the incoming wave-

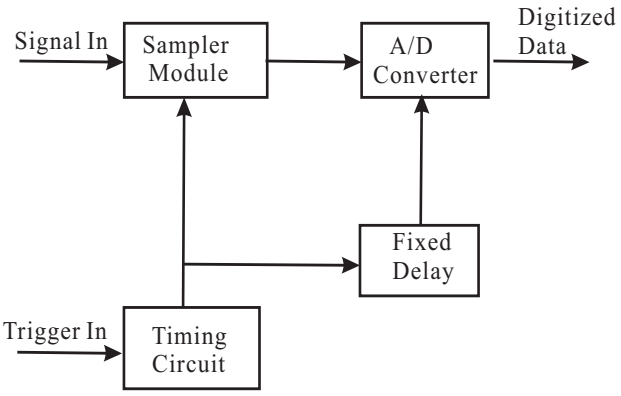

Figure 2.4: Block digram of a sequential equivalent time sampling system

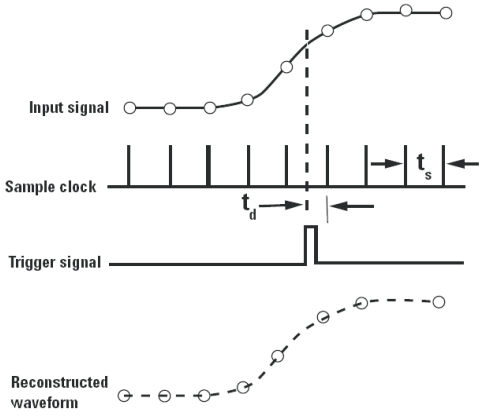

Figure 2.5: Real time sampling process

form's amplitude reaches a certain threshold. At this point that the sampling and digitizing module starts converting the analog waveform to digital data points at a rate asynchronous and unrelated to the input waveform's repetition rate. The conversion rate, know as the sampling rate is typically derived from an internal clock signal. A higher sample rate can be obtained by utilizing the interleaving technique, which increases the effective sampling rate by combing the outputs of two or more ADCs.

2.2.3 Comparisons

The performances of a UWB time domain system with equivalent-time sampling and that with real time sampling are compared below from aspects of measurement accuracy, measurement speed, system cost and etc.

Measurement accuracy

A UWB time domain system with equivalent time sampling has higher accuracy than that with real time sampling. First, an equivalent time sampling system can have higher effective sampling rate than a real time sampling system. The time interval resolution of a high performance time domain measurement system with equivalent sampling, i.e. a sampling oscilloscope, is as small as 62.5 femtoseconds (fs) [67], which corresponds to an effective sampling rate of 16 Terasamples/s, while the fastest time domain system with real time sampling on the market has a sampling rate of 80 Giga-samples per second (Gsps)[68]. A higher sampling rate results in a smaller aliasing error. Second, ADCs used in equivalent time sampling systems generally have a resolution more than 12 bits, while a high speed ADC in a real time sampling system has a resolution less than 8 bits, which produces a larger quantization noise. Third, the thermal noise level and nonlinearity distortion in an equivalent time sampling system are also lower than those of a real time sampling system due to the more mature technology.

Measurement speed and system cost

A UWB time domain system with equivalent time sampling technique reconstructs one waveform from several repetitive measurements and the measurement time is determined by the sampling rate and the number of sampling points. It takes 2 milliseconds (ms) to obtain 2000 samples by using the equivalent time sampling technique if the sampling rate is one Mega-samples per second (Msps). With a real time sampling system, such a measurement takes only fifty nanoseconds (ns) if the sampling rate is 40 Gsps. Therefore, an UWB time domain system with equivalent time sampling technique gives higher measurement accuracy at the cost of measurement speed. However, the cost of an equivalent time sampling system is much cheaper, about 20% of that of a real time sampling system [69], in which very expensive ADCs are used.

Other aspects

An UWB time domain measurement system with equivalent time sampling technique has a complex timing circuit for generating an accurate clock signal. In principle, a real time sampling system can have a very simple system structure. However, as aforementioned, due to the lack of ultra-high speed ADCs, current systems based on real time sampling have several ADCs working in parallel, which also have complicated structures and sophisticated timing circuits [66].

For an UWB time domain system based on equivalent time sampling, a measured signal need to be repetitive within millisecond or longer and this

restricts its use for the detection of high rate biological activities. With the development of solid-state technologies, the cost of a system based on real time sampling will decrease, and its measurement accuracy will also increase, together with the simple system structure, the time domain system based on real time sampling will be more and more attractive for the clinical applications.

Chapter 3

Accuracy of Time Domain Systems

The main concern when using a time domain system instead of a frequency domain system for microwave imaging is the measurement accuracy. In general, a time domain system has a higher noise level in comparison to a frequency domain system, and this could lead to significant degradation in the imaging quality.

In this chapter, the accuracy of time domain systems is investigated. Error sources are identified and classified. Common accuracy characterizations are described.

3.1 Error source

The measurement accuracy of a UWB time domain measurement system is limited by a number of different error sources. These error sources are described below.

3.1.1 Deterministic error

There are two major sources of deterministic error in a time domain system. The first is the error caused by both vertical (voltage) and horizontal (time base) gain. The vertical error is calibrated by applying known DC voltage to the system sampler [70]. The horizontal deterministic error is known as time base distortion and it has a certain regularity. This regularity can be found through reference measurements [65], [71] and used to correct measured data.

The second major source of deterministic error is the waveform distortion effect due to the non-ideal characteristics of the wideband sampling module

and the front-end components. If these components were perfect they would acquire a sample of the measured pulse exactly equal to the voltage of the (continuous) pulse at the desired instances in time. The result would be that the recorded sequence of numbers, representing the pulse wave form, would be described with a convolution between the continuous waveform and a train of equally space impulse functions. In practice, the components used in the time domain system are never perfect and thus the effective impulse response is not a perfect impulse function. This means that the RF front-ends introduces amplitude and phase distortion to the signal. In addition, rather than sampling the measured pulse at instants in time, the sampler samples over a short (nonzero) time interval for each sample. This nonzero sampling "gate" time has the effect of distorting (smoothing out) the fast changing portions of the recorded waveform and thus acts as a low-pass filter in front of an otherwise perfect sampler. All these effects make the obtained signal different from the true one.

The distortion effect of the recorded waveform due to the imperfect system impulse response can be described by the following equation:

$$y(t) = \sum_{n=0}^{N-1} x(nT)h(t - nT) \tag{3.1}$$

where $y(t)$ is a distorted estimate of the sampled waveform $x(nT)$, which represent the continuous function $x(t)$ with sampling interval T. $h(t)$ is the true impulse response of the sampling module. It becomes apparent that, in order to reconstruct the true sampled waveform $x(t)$ from the distorted recorded waveform $y(t)$, the effective impulse response must be known and a method must be devised for deconvolving it from $y(t)$. Two common approaches for obtaining the effective impulse response of the system are by using a pulse standard [72], [73] and by employing the "nose-to-nose" method [74].

Deconvolving the estimated impulse response from the measured waveform is not a trivial problem, as the measured waveforms are corrupted by noise. Deconvolving $y^{'}(t)$ and $h(t)$ is the discrete equivalent of solving an integral equations of the first kind. Several different approaches to this problem have been proposed that are either general or directed specifically to the problem of ultra-wideband time domain system deconvolution [75]–[77].

3.1.2 Random error

Random errors are also present in both vertical and horizontal axis. The vertical part consists of thermal noise from system circuits and quantization noise produced in the digitizing process. Noise resides in the horizontal

(time) channel in the form of timing jitter. Jitter is the undesired deviation from expected sampling instants and this effect could cause big problems in the measurement of a time domain signal. Depending on the measured signal's bandwidth, a slight variations in the timing may seriously degrade the measurement SNR. Fig. 3.1 illustrates the timing jitter effect. In this figure, $u(t)$ is the sampled signal, T_j is the expected sampling instant and the real sampling instant is in the range of $T_j \pm \Delta t_j$.

The way the random errors affect a measurement can be model mathematically. We assume a noise free signal $x(t)$, then the ith sample of the real measured signal, y_i, can be expressed as follows due to the presence of random errors:

$$y_i = x(T_i + \tau_i) + \varepsilon_i + \gamma_i, \tag{3.2}$$

Here $T_i = (i-1)T_s$ is the target time of each sample, T_s is the target time interval between samples. τ_i is the random timing jitter error, ε_i is the thermal noise and γ_i is the quantization noise. The jitter and thermal noise are assumed to be normally distributed and are zero-mean random variables with variances σ_τ^2 and σ_ε^2. Quantization noise is characterized by the least significant bit (LSB) and it is a random process uniformly distributed in the range from -1/2 LSB to 1/2 LSB.

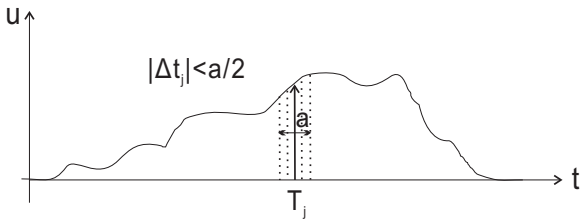

Figure 3.1: The illustration of the timing jitter effect.

Additive signal averaging is routinely used during waveform acquisition to reduce the effects of vertical channel noise. It is usually assumed that, upon averaging, the jitter acts as a lowpass filter [78], so the average of the signals affected by timing jitter is the convolution of the jitter free signal $x(T_i)$ and the probability density function (PDF) $p(t)$ of the jitter, i.e.,

$$\langle x(T_i + \tau_i) \rangle = \int x(T_i - t)p(t)dt \tag{3.3}$$

The effect of timing jitter is thus compensated by deconvolving the jitter probability density function from the recorded waveform data [78], [79]. The approaches described in these two publications for obtaining the jitter PDF are difficult to implement and a much simpler method for calculating

the jitter PDF is proposed in [80]. According to this paper, the frequency spectrum of the jitter probability density function $P(f)$ can be determined from the jitter standard deviation σ_τ:

$$P(f) = e^{-0.5*(2\pi f\sigma_\tau)^2} \tag{3.4}$$

Once $P(f)$ is obtained, the effects of jitter can be removed by deconvolving according to Eq. (3.3).

3.1.3 Nonlinearity

The nonlinearity of a time domain system is mainly caused by amplifiers and sampling circuits. Amplifiers, mainly power amplifiers and low noise amplifiers (LNAs), are often used in order to improve system's signal to noise ratio (SNR). Power amplifiers are strongly nonlinear, which usually degrade the performance of a communication system. A lot of work has been done on modeling and removing the nonlinearity effects of power amplifiers. As power amplifiers are generally used in the transmitting part of the system, the introduced nonlinearity creates no problem to microwave imaging since the objective of microwave imaging is to extract the object response instead of recovering the transmitted signal. Therefore, we are only interested in the nonlinearity introduced by weakly nonlinear components, such as a LNA and sampling circuits.

There are two main approaches for analyzing weakly nonlinear circuits: power-series analysis and volterra-series analysis. The former is equivalent to the latter in the case of memoryless transfer nonlinearities, that is, the current value of the output does not depend on previous values of the input. Although the assumption that circuits contains only ideal memoryless transfer nonlinearities is often unrealistic, the power-series approach gives a good approximation of the behavior of many types of weakly nonlinear components. Therefore, it will be used to study the nonlinearities of UWB pulses.

Many nonlinear circuits are modeled as a frequency-selective network followed by a memoryless broadband transfer nonlinearity [81], as shown in Fig. 3.2.

The nonlinear function $f(u)$ is a polynomial power series:

$$f(u) = \sum_{n=1}^{N} a_n u^n(t) = a_1 u(t) + a_2 u^2(t) + a_3 u^3(t) + ... \tag{3.5}$$

where $u(t)$ is the output of the frequency selective network, a_n (n = 1, 2,...N) are nonlinear coefficients and N is usually limited to three in practice.

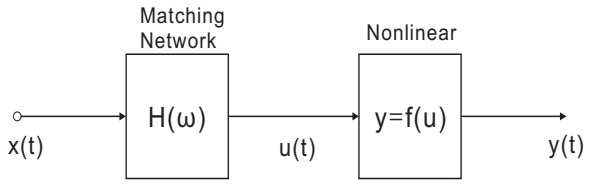

Figure 3.2: The model of a nonlinear circuit.

For a circuit component with flat response, the nonlinearity coefficients can be determined from the gain and intermodulation intercept points [81], which is theoretical power level at which the power of the desired tone and the nth-order (where n is odd) intermodulation product intersect. The nonlinearity error can be made very small by choosing components with good linear performance.

3.1.4 Other errors

Apart from deterministic and random errors, there are also other errors existing in a time domain system. One common type of error is the aliasing error due to finite sampling. Aliasing error occurs because the spectrum of a waveform sampled at time intervals T will be periodic at frequency intervals of $f_0 = 1/T$. If T is not small enough, the aliases of the spectra can overlap with the original spectrum and cause errors. The sampling interval of a sampling oscilloscope can be less than picosecond, which makes the aliasing error negligible. However, the sampling interval obtained from a real time sampling system is much bigger and the aliasing error may become a problem. Time drift is another error which need to be considered when a measurement takes too long time.

3.2 Accuracy characterizations

There are several ways of describing measurement accuracy and the most relevant description might differ for different measurement cases. Important parameters for characterizing the measurement accuracy due to random errors and deterministic errors are described below.

3.2.1 Dynamic range

Dynamic range is extremely important when characterizing many types of microwave devices, and in some cases the key factor in determining measurement performance. Dynamic range describes the range of the input signal

levels that can be reliably measured simultaneously, in particular the ability to accurately measure small signals in the presence of other large signals.

The largest signal amplitude that can be measured is always limited in a digital acquisition system. And the limitation is set by the full scale signal of the system, usually the ADC full scale signal. The analysis of a small signal is on the other hand limited by two other independent error signals: system noise floor and spurious signals. The dynamic range is thus limited by these effects, that give an upper and a lower limit of the detectable signal.

For a system with good linearity, the dynamic range is usually referred to system noise floor. The noise floor sets the minimum power level that the instrument can measure. The noise floor can be lowered by using averaging, or by reducing the system bandwidth (IF BW), which consequently results in a larger dynamic range.

In a frequency domain measurement system, the dynamic range can be easily quantified by taking the ratio between the signal power and noise power. In a time domain measurement system, the dynamic range is usually determined by taking the ratio of the Fourier transform of the generator waveform to the Fourier transform of the noise of the measurement system [82].

$$\text{Dynamic range} = 20\log_{10}\frac{\text{FFT}[Generator(t)]}{\text{FFT}[Noise(t)]} \tag{3.6}$$

where FFT denotes fast Fourier transform.

Although dynamic range is an important performance parameter for many measurement devices, it does not effectively characterize the accuracy of a time domain system for microwave imaging. For example, in a time domain microwave imaging system, the received signals are completely different from the transmitted pulse due to the antenna and propagation effects, therefore, the dynamic range defined in the above equation can not well characterize the measurement accuracy of the imaging system.

3.2.2 Measurement uncertainty

The purpose of a measurement is to determine the value of a quantity of interest. In general, when one repeats a measurement many times, one will obtain many different answers. This variability arises due to the presence of random error sources. Given the inherent variability of a measurement, a statement of a measurement result is incomplete(perhaps even meaningless) without an accompany statement of the estimated uncertainty of measurement.

Measurement uncertainty is a parameter, associated with the result of a measurement, that characterizes the dispersion of the values that could

reasonably be attributed to the quantity subject to measurement [83]. This parameter is a standard deviation which is usually derived from the statistical analysis of experimental data under repetitive conditions. In this condition, independent test results are obtained with the same method on identical test items in the same laboratory by the same operator using the same equipment within short intervals of time.

The standard deviation of time domain measurements under repetitive conditions is calculated as following:

$$\sigma_{Rep}(f) = \sqrt{\frac{1}{N}\sum_{i=1}^{N}(X_i(f) - \overline{X(f)})^2} \tag{3.7}$$

N is the number of repeated measurements, $X_i(f)$ is the fast fourier transform (FFT) of the acquired waveform of index i. $\overline{X(f)}$ is the average of the FFT of all acquired waveforms. $X_i(f)$ and $\overline{X(f)}$ are either amplitude in volts or phase in degrees. As a result, $\sigma_1(f)$ and $\sigma_2(f)$ represent the uncertainties of spectral amplitudes and phases respectively.

The measurement uncertainty is usually expressed in log scale and it has the following relationship to the signal to noise ratio (SNR):

$$\sigma_{dB}(f) = 20\log_{10}[1 + 1/\mathrm{SNR}(f)] \tag{3.8}$$

Here σ_{dB} is the amplitude uncertainty in dB, and $\mathrm{SNR}(f) = \overline{X(f)}/\sigma_1(f)$.

Measurement uncertainty indicates the closeness of agreement between successive results of measurements that are usually made under essentially the same conditions. According to the above equation, it is dependent of not only the system noise level, but also the received signal level, therefore is an appropriate parameter to describe the measurement accuracy of a microwave imaging system.

3.2.3 Measurement bias

The two performance parameters described above says nothing about any deterministic errors that may also be present in the measurement system. Due to this reason, measurement bias is put forward for assessing the size of the systematic error.

Bias is the difference between the expectation of the measured results and accepted reference values, which can be defined with the equation:

$$\Delta = |\overline{X_m} - X_{ref}| \tag{3.9}$$

where $\overline{X_m}$ denotes for the averaged measurement result and X_{ref} is the reference value.

Bias is used for describe the total deterministic error. There may be one or more deterministic error components contributing to the bias. A larger systematic difference from the accepted reference value is reflected by a larger bias value. The result measured by using a high performance system is commonly used as the accepted reference value for evaluating the measurement bias.

Measurement bias can be reduced by means of calibration, which is usually a routine procedure in a microwave imaging system.

Chapter 4

System Development

One of the main goals of this thesis is to develop a time domain system dedicated to medical imaging. It is necessary to consider several different design parameters, such as the frequency range of interest, required accuracy, measurement speed, system cost and if there are circuits already commercially available. In this thesis these factors have been analyzed and a system design is proposed. Based on this design, a prototype has been developed and its performance has been experimentally evaluated.

In this chapter, the design, development and performance tests of the time domain system are presented.

4.1 Design challenges

Considering the spatial resolution and signal penetration depth in biological tissue, the frequency range of interest in our work is from a few hundred megahertz to about 3 GHz.

The generation of ultra short pulses (with bandwidth of several gigahertz) has become possible due to the fast development of advanced solid-state technology. It is mainly the fast and accurate acquisition of UWB data that poses the largest technical challenges.

Such a wideband measurement is preferably made in real time with a wideband, high rate ADC. The limitation to this approach is that current ADCs do not usually have sufficient bandwidth and sampling rate for this very wideband application. According to Nyquist sampling theorem, the sampling rate has to be at least twice of the bandwidth of the sampled signal. High speed ADCs commercially available, however, generally have an analog bandwidth of a few hundred megahertz and a sampling rate of a few hundred mega-samples per second, which are insufficient for the real time acquisition

of a UWB pulse used for medical imaging. For example, a sampling rate of at least 6 Gsps is needed in order to measure the frequency band of interest for tomographic imaging. In addition, maintenance of good sampling linearity at frequencies above the UHF band is technologically challenging and most current ADCs suffer rapidly degrading linearity above gigahertz.

In order to expand the bandwidth, a wideband T/H is employed before the ADC. As to the sampling rate, an equivalent time sampling technique is used in order to achieve a sufficient sampling rate. This sampling method reconstructs signal from several measurement cycles and consequently requires that the measured signal is repetitive. For a medical imaging problem such as breast cancer detection and brain imaging, biological activities usually cause little problem to the imaging results. Therefore, the object response can be assumed to be repetitive during the measurement time of interest.

4.2 Prototype design

Considering the system requirements, such as the frequency range of interest, measurement speed and system cost, and the current technology limitations, we proposed a time domain system suitable for medical applications. The system is designed to be based on off-the-shelf components and the simplified block diagram is given in Fig. 4.1. It includes a pulse generator, a pair of transmitting and receiving antennas, a wideband T/H amplifier, an ADC, a FPGA and a timing circuit. The input bandwidth of the T/H is 4.5 GHz and the maximum sampling rate is 3 Gsps [84]. The ADC's analog bandwidth is 800 MHz and the maximum sampling rate is 250 Msps [85].

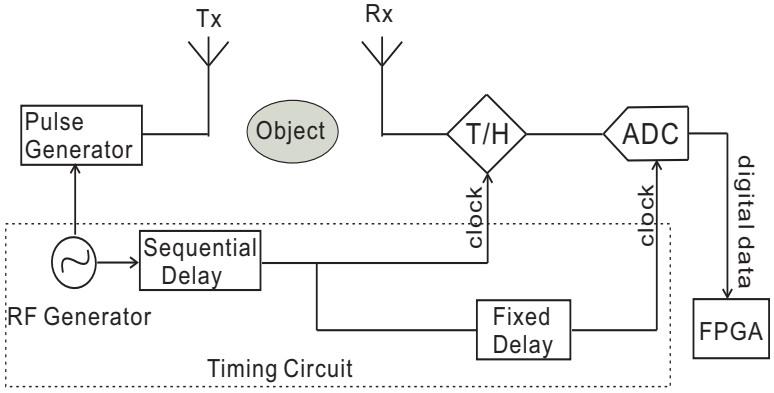

Figure 4.1: The simplified block diagrams of the designed time domain system for medical imaging.

The timing circuit is the crucial part of the system and it is responsible for

Table 4.1: Components/Equipments used in the prototype

Components/Equipments	Model	Manufacturer
T/H (evaluation board)	HMC660LC4B	Hittite Microwave
ADC (evaluation board)	ADS41B29	Texas Instruments
DDS (evaluation board)	AD9959	Analog Devices
PA (evaluation board)	ZHL-42W	Mini-Circuits
AWG	7102	Tektronix
Synthesizer	E8251A	Agilent
FPGA (evaluation board)	ML605	Xilinx

generating accurate clocks to trigger the T/H and the ADC. As mentioned before, an equivalent time sampling method is used, therefore the sampling clocks must be sequentially delayed for every measurement cycle. In addition, there is a fixed propagation delay between the T/H and ADC, and this delay must be taken into account in order to make the ADC sample and digitize at the settled stage of the T/H output.

A prototype has been developed and the block diagrams of the prototype is given in Fig. 4.2. An arbitrary waveform generator (AWG) is used for pulse generation, and the pulse shape can be easily programmed. A wide-band power amplifier (PA) is used to increase the transmitted power. A direct digital synthesizer (DDS) is employed to generate sampling clocks. The frequency and phase offset of the DDS output clocks can be tuned with very fine resolution. A synthesizer is used to provide synchronization between the DDS and the AWG. A clock generated by the AWG is fed to the FPGA in order to control the initial timing for the data recording. The use of the lab equipments facilitates the tests of the developed prototype and they will be later on replaced by self-designed or off-the-shelf components in order to make the full system customized. The components/equipments used in this prototype are listed in Table 4.1 and the off-the-shelf components used in the prototype are shown in Fig. 4.3.

With the developed prototype, an pulse generated by the AWG is firstly

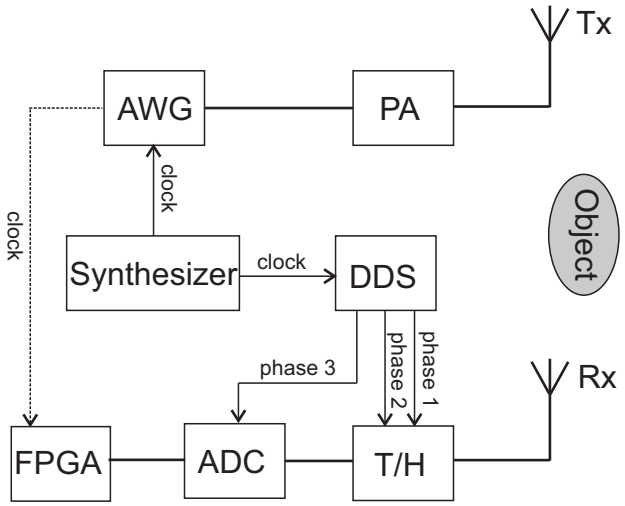

Figure 4.2: The block diagrams of the developed prototype

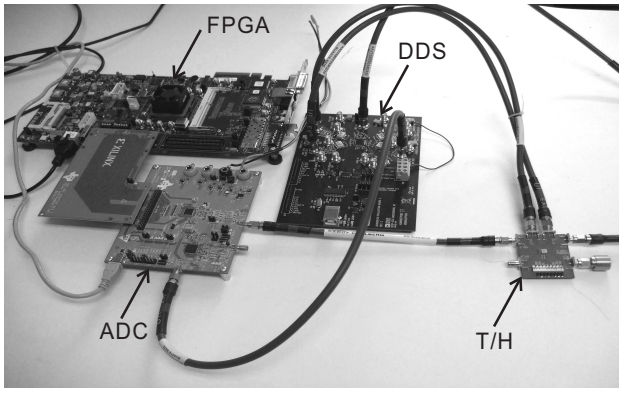

Figure 4.3: The off-the-shelf components used in the prototype.

amplified by the power amplifier(PA) and then transmitted into the object under test by the transmitting antenna. The scattered signal acquired by the receiving antenna is measured by the T/H-ADC assembly. The DDS generate three clock signals with the same frequency but different phases, named phase 1 phase 2 and phase 3 respectively, for triggering the T/H and the ADC. Phase 1 and phase 2 are out of phase, and phase 3 must be well tuned relative to phase 1 and phase 2 in order to make the ADC sample the settled stage of the T/H output. The digital output of the ADC is transferred to the FPGA board and subsequently saved in a PC. The synthesizer provide reference clocks to both the DDS and the AWG, which ensures the clock synchronization for the measurement.

4.3 Sampling algorithm

The generation of a stable and fine delay is crucial for an equivalent time sampling system. Conventional methods use fast ram and staircase generator or delay vernier for delay generation [86], which is complicated to implement and also leads to non-linear time axis representation, and time drift. Thanks to the advancement of solid state technology, there are also commercially available programmable delay chips, which consist of hundreds of delay gates. As these gates are not absolutely identical, the equidistant sampling can not be ensured.

Here, we proposed a simple equivalent time sampling algorithm. In this algorithm, the sequential delay is generated by utilizing the difference between the sampling frequency and the pulse repetition rate. The principle of generating the sequential delay can be explained by the following equation:

$$\delta_t = \frac{N}{f_s} - \frac{1}{f_{rep}} \tag{4.1}$$

where δ_t is the sequential delay resolution, f_s and f_{rep} are the sampling frequency and pulse repetition rate respectively. N is a integer parameter, which is used to tune the time resolution.

With this approach, one sample is taken in each wave cycle and samples are taken at different positions in different cycles. In order to implement this algorithm, f_s and N need to be properly chosen in relative to the repetition frequency. DDS generated clock has a frequency resolution of 0.12 Hz [87], which can give a fine time delay based on the above equation. For example, for a repetition rate $f_{rep} = 10$ MHz, if we choose $f_s = 99.99$ MHz and N = 10 (which means that during the data recording process, only one sample is stored in every ten samples), then the resulted time resolution is about 10 ps.

4.4 System evaluation

The performance of the developed prototype is investigated by using the measurement setup in Fig 4.4. A one volt peak to peak pulse generated by the AWG is measured by the T/H and ADC assembly. The repetition rate of the pulse is 10 MHz and the sampling clock is 99.99 MHz. We choose N = 10 in order to avoid interleaving the samples, and only one sample is stored for each wave cycle.

Fig. 4.5 (a) shows a plot of the output pulse recorded by a 50 GHz, high performance oscilloscope HP 54750A and in Fig. 4.5 (b) the signal obtained from the prototype. It can be seen that the duration of the pulse

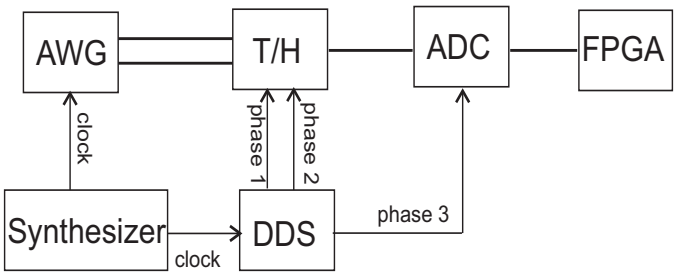

Figure 4.4: The measurement setup for system performance investigation.

increases(pulse broadening phenomenon) due to the bandwidth limiting effect of the prototype.

The system's transfer function is calculated as the ratio of these two signals in frequency domain:

$$TR(f) = \frac{X_{out}(f)}{X_{in}(f)} \tag{4.2}$$

where X_{in} and X_{out} are the frequency spectrum of the input signal and output signal of the receiver, as shown in Fig. 4.5 (a) and (b) respectively.

Fig. 4.6 shows the transfer function and it looks different from the ideal sampling transfer function of the T/H [84]. The result suggests a 3 dB bandwidth of about 3.5 GHz, which covers the frequency range of interest for tomographic imaging.

The measurement accuracy is characterized by the SNR as defined in Eq. (3.8). With the same measurement setup, repetitive measurements were carried out in order to calculate the SNRs and the results are plotted in Fig. 4.7 when the number of average $\text{AVG}_N = 1$ and 16 respectively. The results indicate a large noise component close to 1 GHz, which gives a much lower SNR. In the ideal case, the SNR increases with the square root of the number of average[88], which would results in a 12 dB difference in the SNRs before and after the averaging. However, it can be seen that the results do not follow such a relationship, which suggest the effect of the timing jitter.

Fig. 4.8 shows a comparison of the full scale SNR with those of a VNA, and a time domain experimental system composed of a pulse generator and a sampling oscilloscope [34]. The results show that the SNR difference between the prototype and the VNA is about $10 \sim 20$ dB in the frequency range of interest. It can also be seen that a higher full scale SNR can be obtained using the prototype in comparison with the time domain experimental system. The UWB pseudo-noise device mentioned in the introduction is claimed to have the performance of a network analyzer [52]. Our prototype, on the other

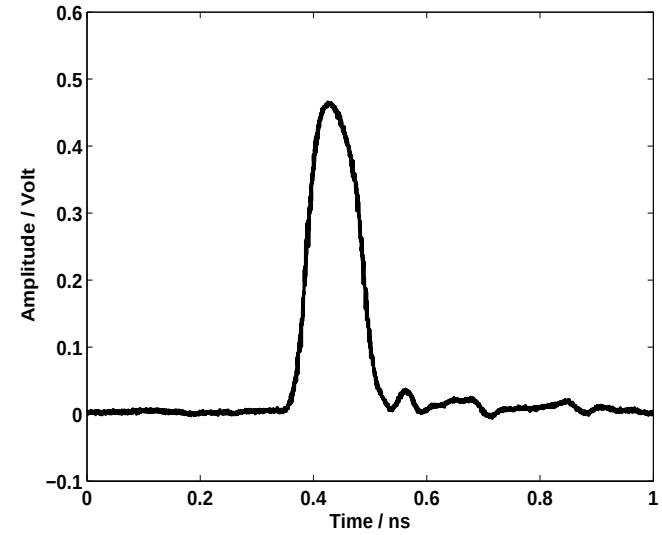

(a)

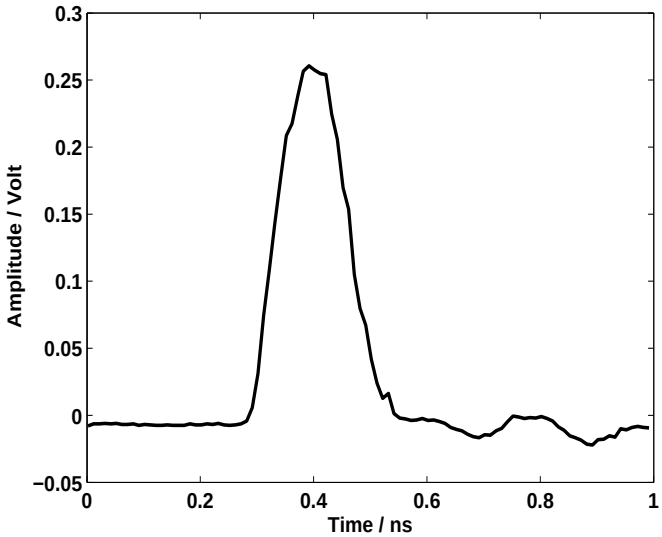

(b)

Figure 4.5: AWG generated pulse measured by (a)a sampling oscilloscope and (b) the developed prototype.

hand, has a much simpler system structure and it can be used for range-gating which the UWB pseudo-noise system is incapable of.

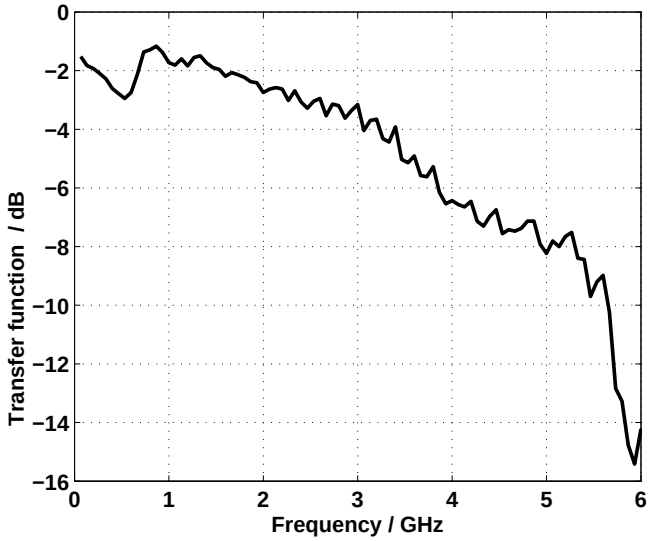

Figure 4.6: The transfer function of the developed system.

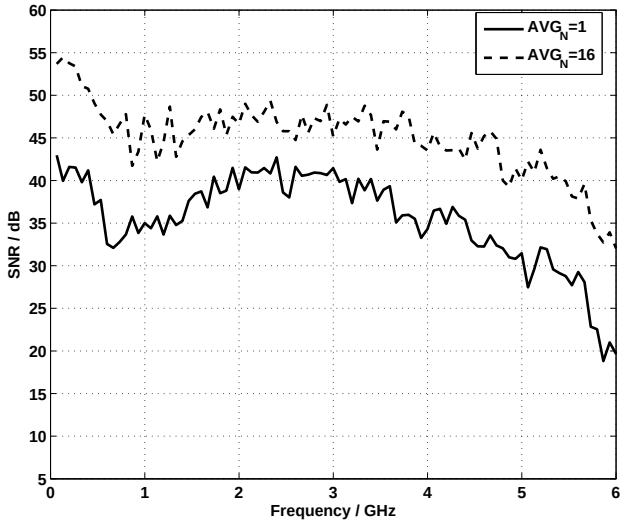

Figure 4.7: The measurement SNRs of the developed prototype when the number of average is $\mathrm{AVG}_N = 1$ and 16 respectively.

4.5 Imaging results

In order to test the function of our system, an imaging test was performed. A two dimensional antenna array composed of twenty monopoles was used

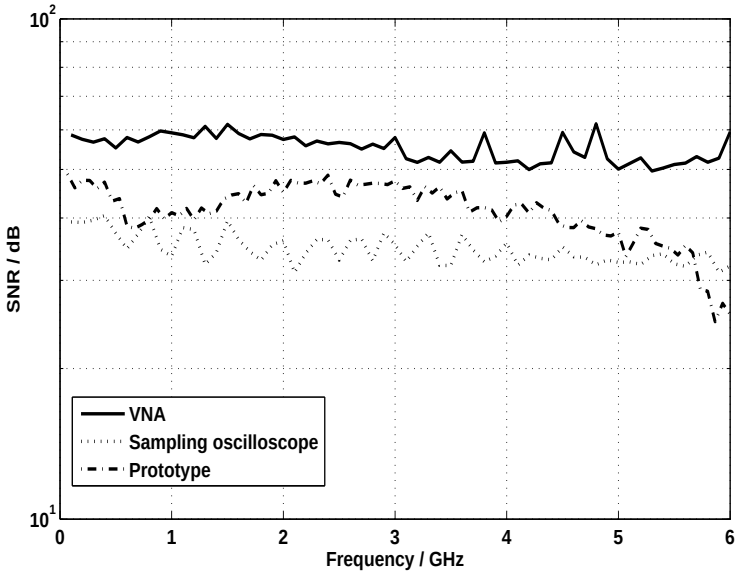

Figure 4.8: The full scale SNR of the prototype in comparison with those of a VNA, and a time domain experimental system composed of a pulse generator and a sampling oscilloscope. The solid line, dashed line and dash-dot line represent the SNRs of the VNA, the time domain experimental system and the prototype respectively.

for signal transmitting and receiving[34]. The twenty antennas were evenly distributed in a circle with a radius of ten centimeters and a plastic cup of oil was put in the center of the imaging region surrounded by the antenna array. The plastic cup was cylindrical-shaped, but with gradually increasing radius. The bottom diameter and top diameter of the cup were 55 mm and 75 mm respectively.

A mechanical switching matrix was employed to select different transmitting and receiving antenna pairs. Measurements were performed according to the measurement procedure described in [34]. Two groups of 20$\times$ 19 data sets were obtained when the number of average in the measurements was $\mathrm{AVG}_N = 1$ and 16 respectively. The same measurements were taken for an empty antenna system without the phantom, in order to carry out the calibration procedure of reconstructions [7].

The tomographic images of the investigated object were shown in Fig. 4.9 and Fig. 4.10 when different spectral content were used. In order to evaluate the imaging quality, imaging results based on measurements with a VNA was used for comparison. The images obtained by using these two different

systems are very similar. This results demonstrate imaging functionality of the developed system.

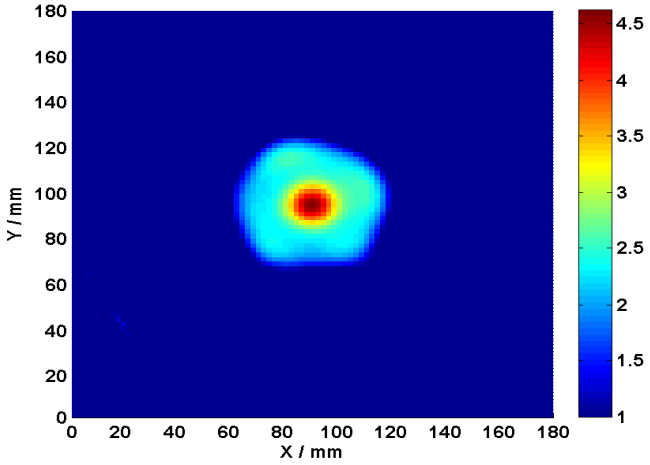

(a)

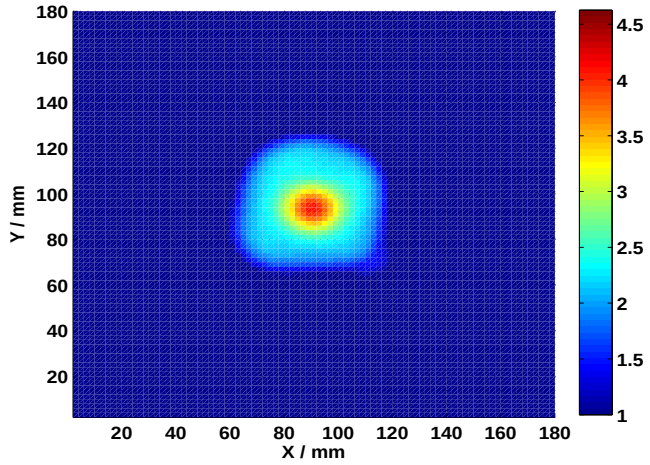

(b)

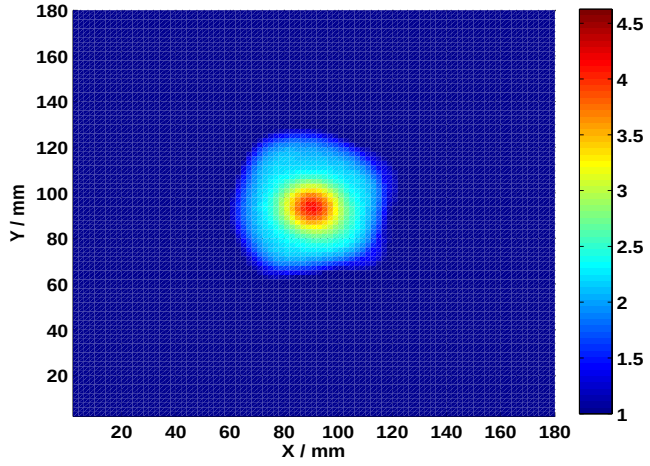

(c)

Figure 4.9: The imaging results obtained by using (a)VNA based experimental system, and (b) (c)the developed prototype when AVG$_N$=1 and 16 respectively. The spectral content used in the reconstruction is centered at 3GHz with 1GHz bandwidth.

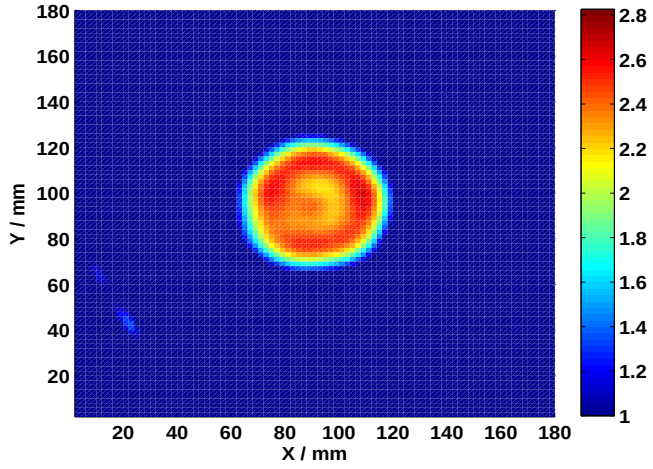

(a)

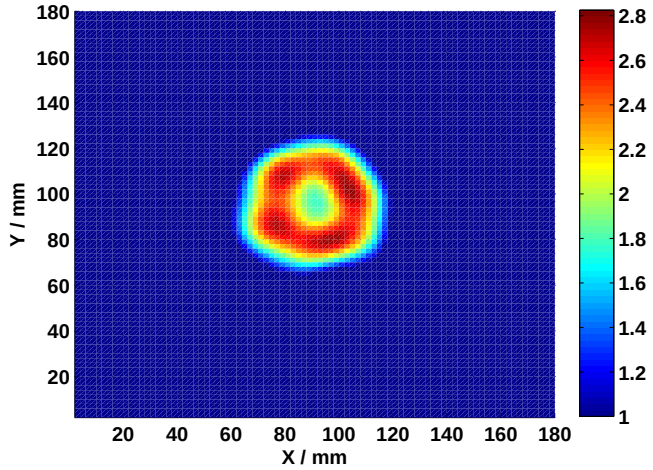

(b)

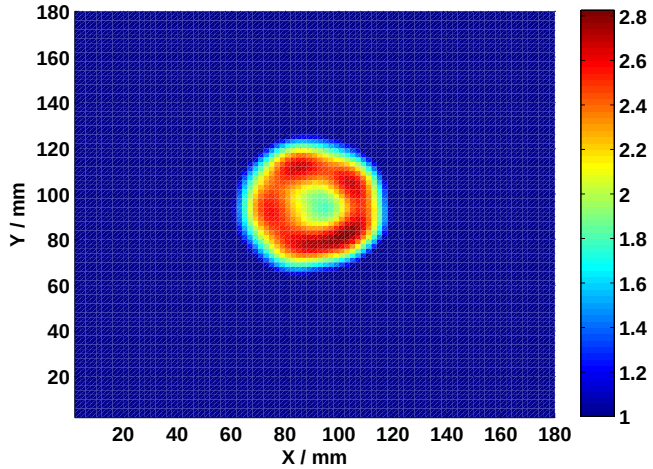

(c)

Figure 4.10: The imaging results obtained by using (a)VNA based experimental system, and (b) (c)the developed prototype when AVG$_N$ =1 and 16 respectively. The spectral content used in the reconstruction is centered at 3GHz with 3GHz bandwidth.

Chapter 5

Summary of Results

In this chapter a brief summary of each paper included in the thesis is given.

5.1 Summary of paper A

In this paper we investigated the measurement accuracy of a simple time domain system and the required measurement accuracy for medical applications.

Theoretical analysis was performed to estimate the accuracy of a time domain system. A specific real time sampling system was studied and the analytically obtained measurement uncertainty were compared with simulated results. Eq. (6) and (7) in the paper give the calculation of amplitude uncertainty and phase uncertainty respectively. In Fig. 3 in the paper the agreement between analytical estimates and simulated results were shown.

The required measurement accuracy for breast tumor detection was investigated by studying the effects of noise on the image reconstruction. A high contrast breast model, shown in Fig. 4 was considered. Fig. 5 gave the noise free reconstruction. Using the same settings as the noise free reconstructions, noise were added to the amplitude and phase of the signals in order to simulate the effects of measurement uncertainty. A relative reconstruction error as function of amplitude uncertainty and phase uncertainty was plotted in Fig. 6. The results were obtained from five individual simulations and a larger variation of the relative reconstruction error can be observed as the amplitude error becomes larger. Fig. 7 shows reconstructed images when a specific level of measurement uncertainty was used in the reconstructions. The results suggested that the effects of measurement errors on the reconstructed images were were practically non-visible when the amplitude uncertainty and phase uncertainty of measured data were lower than 1.5 dB

and 15 degrees, respectively.

5.2 Summary of paper B

Experimental studies were performed in order to investigate the capability of time domain systems for microwave imaging. A time domain system composed of a pulse generator and a sampling oscilloscope was investigated, compared and contrasted to a UWB frequency domain system (a commercial vector network analyzer). Simple measurement setups were developed in order to estimate the measurement uncertainty of the time domain system and the frequency domain system. The results were shown in Fig. 4 and Fig. 5 respectively. The results showed that by averaging 64 measurements, the time-domain system could reach the same level of measurement accuracy as the frequency-domain system in the frequency range of interest. According to the results, a very advantageous feature of the frequency domain system is that the measurement uncertainty does not change much as the signal level, which does not hold for the time domain system. This is very important for microwave imaging, since signals received in a practical imaging system have a large variation in amplitude. In order to obtain the same feature, a variable gain control amplifier should be employed before the sampling oscilloscope.

In order to demonstrate the influence of measurement accuracy on microwave imaging, a plastic cup of oil was reconstructed with the time domain system and the resulting reconstructions were compared to those obtained by using the frequency domain system. Fig. 8 and Fig. 9 showed the reconstructed permittivity and conductivity profiles respectively. The results showed that the permittivity reconstructions were of better quality than the conductivity. It can be seen that the permittivity profile of the phantom reconstructed from the non-averaging time domain measurements is very similar to that obtained by means of the frequency domain system. This indicates that the time domain system is accurate enough for the imaging of this specific phantom.

In order to investigate the influence of the recording length of time domain data on the reconstructions, a relative reconstruction difference as defined in Eq. (15) is plotted in Fig. 10 as the function of iteration numbers when different recording length were used. The results showed that the reconstruction quality improved as the recording length increased from 12 to 30 ns. The reason is that a recording length of 12 ns was not long enough for collecting the multiple-scattered field of the object. The results also showed that as the recording length was increased further to 50 ns, the reconstruction quality became worse, which could be attributed to unwanted late time-arrival signals,

e.g., scattered signals from the surrounding environment.

5.3 Summary of paper C

In this paper, a time domain system design dedicated to microwave medical imaging was proposed and the system performance was evaluated for a specific imaging scenario based on simulations.

The challenges in designing a time domain system for UWB microwave imaging were discussed. Considering current technology limitations, a system design suitable for UWB microwave imaging was proposed, shown in Fig. 1. The system structure was introduced and the measurement principle was described.

The measurement accuracy of the proposed system was evaluated by means of network analysis and simulations. Both the vertical noise and horizontal noise (timing jitter) were investigated. A specific three dimensional(3D) antenna array, given in Fig. 1 (c), was considered in the evaluation. The signal to noise ratios (SNRs) of measured signals due to vertical noise were shown in Fig. 9 when the antenna array was placed in air. The results suggested that the system had optimal performance around 3 GHz. In order to demonstrate the effects of matching liquid on the system performance, the measurement SNRs were estimated and plotted in Fig. 11 when three different matching liquids were used. The results showed that the use of matching liquids made the measurement SNRs better in the low frequency end. Nevertheless, the SNR difference between the strongest and the weakest signals became larger when a matching liquid was used, this is quite natural but makes it more challenging to measure the weaker signals accurately. The effects of timing jitter were plotted in Fig. 13. It was shown that the effect of the timing jitter of 1$\sim$2 ps on the strongest received signal was comparable to that of the voltage noise.

Based on all the investigations, we concluded that with the presented system, a signal to noise ratio higher than 30 dB was obtained in the frequency range of 500 MHz to 3 GHz when the effective sampling rate is 50 Gsps.

5.4 Summary of paper D

A time domain measurement system for medical imaging was developed and the performance of the developed prototype was investigated.

In the implementation, a novel method of generating equivalent time sampling clock was employed. This method utilized the difference between

the signal repetition rate and the sampling frequency for delay generation, which allowed for a very precise delay resolution. The measurement results showed the efficacy of this method.

The transfer function of the system was calculated and plotted in Fig. 8. The result showed that the 3dB bandwidth of the developed prototype was about 3.5 GHz. The measurement accuracy of the system was characterized by signal to noise ratio, and the SNRs obtained for different cases are calculated and presented in Fig. 9 and Fig. 10 respectively. The results suggested that a SNR over 40 dB can be obtained from about 800 MHz to 3.8 GHz with this system.

An object was imaged with the prototype in order to test its functionality. The same object was imaged with a VNA based experimental system, and the reconstructed image was used as a reference for comparison. Fig. 12 and Fig. 13 show comparisons between the tomographic images obtained with different systems. Comparisons were made when different spectral content were used in the reconstructions. The results showed small difference between the images, which confirmed the functionality of the developed prototype that it is useful in imaging applications.

Chapter 6

Conclusions and Outlook

In this chapter our contributions are summarized and directions for future work are discussed.

6.1 Conclusion

The contributions of this work to the state of the art are mentioned here briefly. There are two main contributions: the accuracy evaluation of time domain systems for medical imaging and a time domain system developed for medical diagnostics.

We have carried out a comprehensive evaluation of the measurement accuracy of time domain systems for medical imaging. The accuracy estimation has been derived and verified, and the effects of measurement accuracy on the image quality has been investigated. Several practical issues in medical imaging, such as antenna performance and propagation effects, have been addressed in the evaluation. Imaging examples showed that the same imaging quality was obtained using a time domain system and a UWB frequency domain system. This part of work was presented in paper A and paper B.

Considering the system requirements and the available technologies, we have proposed a time domain system design dedicated to medical imaging. The performance obtained with the proposed design was evaluated for a specific imaging scenario, and this part of work was presented in paper C. The results suggest that antennas and matching liquid play big roles in determining the measurement accuracy.

A prototype has been developed based on the design, and its performance has been investigated and compared to other commercially available systems. Results show that the measurement accuracy of the prototype falls in between those of the VNA and the time domain experimental system. An imaging

test performed with the prototype proved its functionality for imaging. This part of work was summarized in paper D.

6.2 Future work

The work presented in the thesis was based on theoretical considerations, simulations and experimental tests. There are still many problems need to be solved in the development of a customized medical imaging system. In order to develop a more complete system, further efforts need to be made in the following directions:

6.2.1 Prototype improvement

Some hardware will be replaced in order to give better performance. The T/H used in the prototype does not have the same performance as the specified. A T/H with low noise and clean output would give better system performance. The DDS employed in the system has a relative low sampling rate, which limits the frequency of the output clocks. In addition, the DDS generated clock has a timing jitter of about 2.5 ps RMS [89], which is quite much for our applications. Therefore, the alternative way of generating more precise clocks will be investigated.

6.2.2 Development of a completely customized system

A complete time domain microwave imaging system is composed of a pulse generator, a UWB receiver, an antenna array and a switching system. In this thesis, only the receiver of the presented system is composed of off-the shelf components and other high cost system parts should also be customized.

The pulse generator used in the thesis is a commercial instrument, which has a large size and is very expensive. As mentioned in section 2.2.1, there are several technologies for pulse generator design and many self-designed pulse generator for UWB applications have been reported recently [90]–[91]. Therefore, designing a suitable pulse generator for medical imaging is one of the main objectives for the future. In order to make the signal power mainly distributed in the frequency range of interest, the pulse shape and pulse duration should be carefully chosen.

In addition, the switching system we are using now is of mechanical type, which has a low switching speed and massive size. As the advancement of solid-stage technology, there are many types of electrical switches available.

From these switches, we can develop a suitable switching system, which further reduces the system cost and size of the imaging system.

6.2.3 Adaptive gain control in the system

Based on our investigations, the challenge of making accurate measurement with a time domain system is the large variation in the amplitudes of the received signals. Unlike a VNA, in which measurement accuracy is almost unchanged in a certain intensity range, the time domain system measures weak signals with very poor SNR. In order to improve the measurement accuracy for weak signals, amplifiers are usually employed ahead of the sampling module. This, however, will potentially cause some strong signals to exceed the full scale level of the T/H-ADC assembly. Therefore, a variable gain control scheme must be implemented in order to adjust the system gain adaptively.

6.2.4 System miniaturization

The final goal is to put the entire system on a chip. Once a customized system has been developed with satisfying performance, all components could be integrated into one chip and a very compact and versatile microwave imaging measurement system has been realized.

References

[1] J. C. Bolomey, A. Izadnegahdar, L. Jofre, C. Pichot, G. Peronnet, and M. Solaimani, "Microwave diffraction tomography for biomedical applications," *IEEE Trans. Microwave Theory Tech.,* vol. MTT-30, no.11, pp. 1998–2000, 1982.

[2] C. Pichot, L. Jofre, G. Peronnet, and J. C. Bolomey, "Active microwave imaging of inhomogeneous bodies," *IEEE Trans. Antennas Propagat.,* vol. AP-33, no. 4, pp. 416–425, 1985.

[3] L. Jofre, M. S. Hawley, A. Broquetas, E. de los Reyes, M. Ferrando, and A. R. Elias-Fusté, "Medical imaging with a microwave tomographic scanner," *IEEE Trans. Biomed. Eng.*, vol. 37, no. 3, pp. 303–312, 1990.

[4] P.M. Meaney, M.W. Fanning, D. Li, S.P. Poplack and K.D Paulsen, "A clinical prototype for active microwave imaging of the breast," *IEEE Trans. Microwave Theory Tech.,* vol. 48, no. 11, pp. 1841–1853, 2000.

[5] E. C. Fear and M. A. Stuchly, "Microwave detection of breast cancer," *IEEE Trans. Microwave Theory Tech.,* vol. 48, no. 11, pp. 1854–1863, 2000.

[6] S. Y. Semenov, A. E. Bulyshev, A. E. Souvorov, A. G. Nazarov, and etc., "Three-dimensional microwave tomography: Experimental imaging of phantoms and biological objects," *IEEE Trans. Microwave Theory Tech.,* vol. 48, no. 6, pp. 1071–1074, 2000.

[7] A. Fhager, P. Hashemzadeh, and M. Persson, "Reconstruction quality and spectral content of an electromagnetic time-domain inversion algorithm," *IEEE Trans. Biomed. Eng.,* vol. 53, no. 8, pp. 1594–1604, 2006.

[8] J. E. Johnson, T. Takenaka, and T. Tanaka, "Two-dimensional time-domain inverse scattering for quantitative analysis of breast composition," *IEEE Trans. Biomed. Eng.,* vol. 55, no. 8, pp. 1941–1945, 2008.

[9] M. Klemm, I. J. Craddock, J. A. Leendertz, A. Preece and R. Benjamin, "Radar-based breast cancer detection using a hemispherical antenna array-experimental results," *IEEE Trans. Antennas Propagat.,* vol.57, no. 6, pp. 1692–1704, 2009.

[10] T. S. England and N. A. Sharples, "Dielectric properties of the human body in the microwave region of the spectrum," *Nature*, vol. 163, pp. 487–488, 1949.

[11] R. Pethig, "Dielectric properties of biological materials: Biophysical and medical applications," *IEEE Trans. Elect. Insulation*, vol. EI-19, no. 5, pp.453–474, 1984.

[12] K. R. Foster and H. P. Schwan. "Dielectric properties of tissues and biological materials: A critical review," *Crit. Rew. Biomed. Eng.,* vol.17, pp. 25–104, 1989.

[13] G. Gabriel, S. Gabriel, and E. Corthout, "The dielectric properties of biological tissues: I. Literature survey," *Phys. Med. Biol.,* vol. 41, no. 11, pp.2231–2249, 1996.

[14] S. Gabriel, R. W. Lau and C. Gabriel, "The dielectric properties of biological tissues: II. Measurements in the frequency range 10 Hz to 20 GHz," *Phys. Med. Biol.,* vol. 41, no. 11, pp.2251–2269, 1996.

[15] M. Lazebnik, D. Popovic, L. McCartney, C. B. Watkins, and etc., "A large scale study of the ultra wideband microwave dielectric properties of normal, benign and malignant breast tissues obtained from cancer surgeries," *Phys. Med. Biol.,* vol. 52, no. 20, pp. 6093–6115, 2007.

[16] S. S. Chaudhary, R. K. Mishra, A. Swarup, and J. M. Thomas, "Dielectric properties of normal and malignant human breast tissues at radiowave and microwave frequencies," *Indian J. Biochem., Biophys.,* vol. 21, pp. 76-79, 1984.

[17] A. J. Surowiec, S. S. Stuchly, J. R. Barr, and A. Swarup, "Dielectric properties of breast carcinoma and the surrounding tissues," *IEEE Trans. Biomed. Eng.,* vol. 35, no. 4, pp. 257–263, 1988.

[18] W. T. Joines, Y. Zhang Y, C. Li, and R. L. Jirtle, "The measured electrical properties of normal and malignant human tissues from 50 to 900 MHz," *Med. Phys.,* vol. 21, no. 4, pp. 547–550, 1994.

[19] S. Y. Semenov and D. R. Corfield, "Microwave tomography for brain imaging: feasibility assessment for stroke detection," *International Journal of Antennas and Propagation,* vol. 2008, article ID 254830, 2008.

[20] A. N. Reznik and N. V. Yurasova, "Near field microwave tomography of biological objects," *Technical Physics,* vol, 49, no. 4, pp. 485–493, 2004.

[21] W. C. Chew and J. H. Lin, "A frequency-hopping approach for microwave imaging of large inhomogeneous bodies," *IEEE Microwave Guided Wave Lett.*, vol. 5, no. 12, pp. 439–441, 1995.

[22] O. S. Haddadin and E. S. Ebbini, "Imaging strongly scattering media using a multiple frequency distorted Born iterative method," *IEEE Trans. Ultrason., Ferroelect., Freq. Contrl.,* vol. 45, no. 6, pp. 1485–1496, 1998.

[23] Q. Fang, P. M. Meaney, and K. D. Paulsen, "Microwave image reconstruction of tissue property dispersion characteristics utilizing multiple-frequency information," *IEEE Trans. Microwave Theory Tech.,* vol. 52, no. 8, pp. 1866–1875, 2004.

[24] G. Breed, "A Summary of FCC Rules for Ultra Wideband Communications," *High Frequency Electronics,* pp. 42-44, 2005.

[25] E. C. Fear, J. Sill, and M. A. Stuchly, "Experimental feasibility study of confocal microwave imaging for breast tumor detection," *IEEE Trans. Microw. Theory Tech.,* vol. 51, pp. 887–892, 2003.

[26] L. Xu, S. K. Davis, S. C. Hagness, D. W. van der Weide, and B. D. Van Veen,"Microwave imaging via space-time beamforming: Experimental investigation of tumor detection in multilayer breast phantoms," *IEEE Trans. Microw. Theory Tech.,* vol. 52, no. 2, pp. 1856–1865, 2004.

[27] J. M. Sill and E. C. Fear, "Tissue sensing adaptive radar for breast cancer detection:experimental investigation of simple tumor models," *IEEE Trans. Microw. Theory Tech.,* vol. 53, no. 11, pp. 3312–3319, 2005.

[28] G. Bindu, A. Lonappan, V. Thomas, C. K. Aanandan, and K. T. Mathew, "Acitve microwave imaging for breast cancer detection," *Progress in Electromagnetics Research,* vol. 58, pp. 149–169, 2006.

[29] S. M. Salvador and G. Vecchi, "Experimental tests of microwave breast cancer detection on phantoms," *IEEE Trans. Antennas Propagat.,* vol. 57, no. 6, pp. 1705–1712, 2009.

[30] M. E. Hines and H. E. Stinehelfer Sr., "Time domain oscillographic microwave network analysis using frequency domain data," *IEEE Trans. Microwave Theory Tech.,* vol. 22, no. 3, 1974.

[31] Z. A. Maricevic, T. K. Sarkar, Y. Hua and A. R. Djordjevic, "Time domain measurements with the Hewlett-Packard network analyzer HP8510 using the matrix pencil method," *IEEE Trans. Microwave Theory Tech.,* vol. 39, no. 3, pp.538–547, 1991.

[32] J. C. Y. Lai, C. B. Soh, E. Gunawan and K. S. Low, "UWB microwave imaging for breast cancer detection–Experiments with heterogeneous breast phantoms," *Progress in Electromagnetics Research M,* vol. 16, pp. 19–29, 2011.

[33] F. C. Chen and W. C. Chew, "Time domain ultra-wideband microwave imaging radar system," *J. of Electromagn. Waves and Appl.,* vol. 17, no. 2, pp. 313–331, 2003.

[34] X. Zeng, A. Fhager, P. Linner, M. Persson and H. Zirath, "Experimental investigation of the accuracy of an ultrawideband time-domain microwave-tomographic System," *IEEE Tran. Instrum. Meas.,* vol. 60, no. 12, pp. 3939–3949, 2011.

[35] A. Santorelli, M. Chudzik, E. Kirshin, E. Porter, A. Lujambio, I. Arnedo, M. Popovic, and J. Schwartz, "Experimental demonstration of pulse shaping for time-domain microwave breast imaging," *Progress in Electromagnetics Research,* vol. 133, pp. 309–329, 2013.

[36] W. C. Chew, Waves and fields in inhomogeneous media, *New York: Van Nostrand Reinhold*, 1990.

[37] R. Maini, M. F. Iskander, and C. H. Durney, "On electromagnetic imaging using linear reconstruction techniques," *Proc. IEEE,* vol. 68, no. 12, pp. 1550–1552, 1980.

[38] A. J. Devaney, "Reconstructive tomography with diffracting wavefields," *Inverse Problems,* vol. 2, pp. 161–183, May 1986.

[39] R. Aitmehdi, A. P. Anderson, S. Sali, and M. Ferrando, "The determination of dielectric loss tangent by microwave phase tomography," *Inverse Problems,* vol. 4, no. 2, pp. 333–345, 1988.

[40] M. Slaney, A. C. Kak, and L. E. Larsen, "Limitations of imaging with first order diffraction tomography," *IEEE Trans. Microwave Theory Tech.,* vol. 32, pp. 860–873, 1984.

[41] J. C. Bolomey, C. Pichot and G. Gaboriaud, "Planar microwave camera for biomedical applications: Critical and prospective analysis of recontruction algorithms," *Radio Sci.,* vol. 26, pp. 541–549, 1991.

[42] N. Joachimowicz, C. Pichot, and J. P. Hugonin, "Inverse Scattering: an iterative numerical method for electromagnetic imaging," *IEEE Trans. Antennas Propagat.,* vol. 39, no. 12, pp. 1742–1752, 1991.

[43] T. Isernia, V. Pascazio, and R. Pierri, "A nonlinear estimation method in tomographic imaging," *IEEE Trans. Geosci. Remote Sensing,* vol. 35, no. 4, pp. 910–923, 1997.

[44] A. Abubakar, P. M. van den Berg, and J. J. Mallorqui, "Imaging of biomedical data using a multiplicative regularized contrast source inversion method," *IEEE Trans. Microwave Theory Tech.*, vol. 50, no. 7, pp. 1761–1771, 2002.

[45] Q. H. Liu, Z. Q. Zhang, T. T. Wang, J. A. Bryan, G. A. Yabbara, L. W. Nolte, and W. T. Jones, "Active microwave imaging I – 2-D forward and inverse scattering methods," *IEEE Trans. Microwave Theory Tech.*, vol. 50, no. 1, pp. 123–133, 2002.

[46] Z. Q. Zhang and Q. H. Liu, "Three-dimensional nonlinear image reconstruction for microwave biomedical imaging," *IEEE Trans. Biomed. Eng.,* vol. 51, no. 3, pp. 544–548, 2004.

[47] S. Caorsi, S. Ciaramella, G. L. Gragnani, and M. Pastorino, "On the use of regularization techniques in numerical inverse scattering soluaitons for microwave imaging applications," *IEEE Trans. Microwave Theory Tech.,* vol. 43, no. 3, pp. 632–640, 1995.

[48] www.novelda.no

[49] Y. Yang, C. Zhang and A. E. Fathy, "Development and implementation of ultra-wideband see-through-wall imaging system based on sampling oscilloscope," *IEEE Antennas Wireless propag. Lett.,* vol. 7, pp. 465–468, 2008.

[50] A. Aloisio, R. Giordano, and V. Izzo, "Jitter issues in clock conditioning with FPGAs," *17th IEEE-NPSS Real Time Conference (RT),* Lisbon, May, 2010.

[51] R. Herrmann, "M-sequence based ultra-wideband radar and its application to crack detection in salt mines," Faculty of Electrical Engineering and Information Technology, IImenau University of Technology, IImenau, 2011.

[52] J.Sachs, M. Kmec, R. Herrmann, M. Helbig, and K. Schilling, "Integrated Pseudo-Noise Device with Network Analyzer Performance for UWB Sensing and Component Test," *IEEE International Symposium on Signals, Systems, and Electronics (ISSSE),* vol. 7, pp. 465–468, October, 2012.

[53] M.G.M. Hussain, "Ultra-wideband impulse radar-an overview of the principles," *IEEE Aerospace and Electronic Systems Magazine,* vol. 13, no. 9, pp. 9–14, 1998.

[54] R. J. Sullivan, Radar foundations for imaging and advanced Concepts, *SciTech Publishing*, 2004.

[55] M. Hiebel, Fundamentals of vector network analysis, *ROHDE SCHWARZ*, 2005.

[56] W. F. Egan, Phase lock basics, *WILEY-INTERSCIENCE*, 1998.

[57] R. A. Wannamaker, The theory of dithered quantization, *University of Waterloo*, 2003.

[58] J. R. Andrews, Picosecond pulse generators for UWB radars, *Application Note AN-9*, 2000.

[59] Hewlett-Packard, Pulse and waveform generation with step recovery diodes, *Application Note 918*, 1968.

[60] J. R. Andrews, Picosecond pulse generation techniques and pulser capabilities, *Application Note AN-19*, 2008.

[61] J. S. Lee and C. Nguyen, "Uniplanar picosecond pulse generator using step-recovery diode," *Electronics letters,* vol. 37, no. 8, pp. 504-506, 2001.

[62] J. W. Han and C. Nguyen, "Ultra-wideband electronically tunable pulse generators," *IEEE Microwave and Wireless Components Letters,* vol. 14, no. 3, pp. 112-114, 2004.

[63] C. Zhang and A. E. Fathy, "Reconfigurable pico-pulse generator for UWB applications," *IEEE MTT-S International Microwave Symposium Digest,* pp. 407 - 410, 2006.

[64] Application Note1608, "What is the difference between an equivalent time sampling oscilloscope and a real-time oscilloscope?" *Agilent.*

[65] F. Attivissimo, A. D. Nisio, N. Giaquinto and M. Savino, "Measing time base distortion in analog-memory sampling digitizers," *IEEE Tran. Instrum. Meas.,* vol. 57, no. 1, pp. 55 - 62, 2008.

[66] "Multiply your sampling rate with time-interleaved data converters," *MAXIM*, 2001.

[67] 54750A User's Guide, *www.agilent.com*, 1998.

[68] WaveMaster 8 Zi Series 4GHz - 30GHz–World's Fastest Real-time Oscilloscope, *LeCroy.*

[69] http://www.home.agilent.com/agilent/

[70] W. L. Gans, "Calibration and error analysis of a picosecond pulse waveform measurement system at NBS," *Proceedings of the IEEE,* vol. 74, no. 1, pp. 86-89, 1986.

[71] C. M. Wang, P. D. Hale, and K. J. Coakley, "Least-squares estimation of time-base distortion of sampling oscilloscopes," *IEEE Trans. Instrum. Meas.,* vol. 48, no. 6, pp. 1324-1332, 1999.

[72] W. L. Gans, " Dynamic calibration of waveform recorders and oscilloscopes using pulse standards," *IEEE Trans. Instrum. Meas.,* vol. 39, no. 6, pp. 952–957, 1990.

[73] D. Henderson and A. G. Roddle, "Calibration of fast sampling oscilloscopes," *Meas. Sci. Technol.* vol. 1, pp. 673–679, 1990.

[74] J. Verspecht and K. Rush, "Individual characterization of broadband sampling oscilloscopes with a nose-to-nose calibration procedure," *IEEE Trans. Instrum. Meas.,* vol. 43, no. 2, pp. 347–354, 1994.

[75] N. S. Nahman and M. E. Guillaume, "Deconvolution of time domain waveforms in the presence of noise," *NBS Tech. NOte 1047,* 1981.

[76] T. K. Sarkar, D. D. Weiner, V. K. Jain, and S. A. Dianat, "Impulse response determination in the time domain," *IEEE Trans. Antennas Propagat.,* vol. AP-30, pp. 657–663, 1982.

[77] B. Parruck and S. M. Riad, "Study and performancee evaluation of two iterative frequency domain deconvolution techniques," *IEEE Trans. Intrum. Meas.,* vol. IM-33, no. 4, pp. 281–287, 1984.

[78] W. L. Gans, " The measurement and deconvolution of time jitter in equivalent time waveform samplers," *IEEE Trans, Instrum, Meas.,* vol. IM-32, no.1, pp.126–133, 1983.

[79] J. Verspecht, "Compensation of timing jitter-induced distortion of sampled waveforms," *IEEE Trans. Instrum, Meas.,* vol. 43, no. 5, 1994.

[80] J. R. Andrews, "Removing jitter from picosecond pulse measurements," *Application Note AN-23,* Picosecond Pulse Labs, Boulder, 2009.

[81] S. A. Mass, Nonlinear Microwave Circuits, *ARTECH HOURSE, INC.,* 1988.

[82] P. Ferrari and G. Angennieux, " A simulation technique for the evaluation of random errors effects in time domain measurment systems," *IEEE Trans. Instrum. Meas.,* vol. 50, no. 3, pp. 665–671, 2001.

[83] B. N. Taylor and C. E. Kuyatt, "Guidelines for evaluating and expressing the uncertainty Of NIST measurement results," *NIST Technical Note 1297,* 1994 Edition.

[84] Datasheet of HMC660LC4B. www.hittite.com.

[85] Datasheet of ADS41B29. www.ti.com.

[86] M. Kahrs, "50 Years of RF and microwave sampling," *IEEE Tran. Microwave Theory Tech.,* vol. 51, no. 6, pp. 1787–1805, 2003.

[87] Datasheet of AD9959. www. analog.com.

[88] X. Zeng, A. Fhager, M. Persson, P. Linner and H. Zirath, "Accuracy Evaluation of Ultrawideband Time Domain Systems for Microwave Imaging," *IEEE Trans. Antennas Propagat.*, vol. 59, no. 11, pp. 4279–4285, 2011.

[89] D. Brandon, "Direct digital synthesizers in clocking applications time jitter in direct digital synthesizer-based clocking systems," *AN-823 APPLICATION NOTE*, 2006.

[90] M. Stoopman, W. A. Serdijin, "A sub-GHz UWB pulse generator for wireless implantable medical devices," *IEEE Biomedical Circuits and Systems Conference (BioCAS),* pp. 149–152, 2011.

[91] J. B. Radic, A. M. Djugova, L. F. Nagy, and M. S. Videnovic-Misic, "A low power 3.1–7.5 GHz tunable pulse generator for impulse radio UWB," *2012 IEEE 10th Jubilee International Symposium on Intelligent Systems and Informatics (SISY),* pp. 425–428, 2012.